Published online in Wiley InterScience (www.interscience.wiley.com). DOI: 10.1002/poc.842

Catalytic dehydrogenation of ethane over mononuclear Cr(III) surface sites on silica. Part I. C—H activation by σ-bond metathesis†

Sindre Lillehaug,[1] Knut J. Børve,[1]* Marek Sierka[2] and Joachim Sauer[2]

[1]Department of Chemistry, University of Bergen, Allégaten 41, NO-5007 Bergen, Norway
[2]Institut für Chemie, Humboldt-Universität zu Berlin, Unter den Linden 6, D-10099 Berlin, Germany

Received 25 March 2004; revised 6 June 2004; accepted 10 June 2004

ABSTRACT: Mononuclear Cr(III)–silica models have been studied by quantum chemical methods with respect to catalytic activity toward dehydrogenation of ethane. Both cluster and slab models have been developed and used to explore the conceptual model of mononuclear Cr(III) with three covalent ligands that coordinate through oxygen. The study focuses on a reaction mechanism consisting of three main reaction steps: (1) C—H activation of ethane according to σ-bond metathesis and accompanied by the formation of O—H and Cr—C bonds, (2) β-H transfer to chromium with subsequent loss of ethene and (3) regeneration of the chromium site under evolution of H_2. An alternative mechanism is also explored, in which C—H activation takes place at a reactive hydridochromium complex. Stationary points pertaining to these reactions have been optimized, and free energy calculations are used to identify the rate-determining steps. The influence of the local structure of the chromium surface sites is explored by means of a number of idealized surface models and electronic energy profiles for the reactions. Copyright © 2004 John Wiley & Sons, Ltd.

KEYWORDS: Cr–oxide catalyst; silica; ethane; CH-activation; dehydrogenation; reaction mechanism; DFT; QMMM; cluster

INTRODUCTION

Dehydrogenation has become an increasingly topical method for chemical upgrading of liquid natural gas.[1,2] Both homogeneous and heterogeneous catalytic systems have been developed, and some 7 million metric tons of C3—C4 olefins are anually produced this way.[2] Finely dispersed platinum and oxide-supported chromium[2,3] appear as the most interesting catalysts from an industrial point of view. Chromium shows interesting catalytic activity on alumina, which was the original[4] and still is the most commonly used support, but also on silica, zirconia and titania.[3]

Specific aspects of the preparation of the catalyst affect the activity of chromium in these systems. Chromium is added in the form of a precursor compound, and only after drying, calcination and reduction is the catalyst active.[3] After calcination, chromium is believed to be anchored via oxygen bridges to the substrate.[5–7] At low chromium load on silica, mononuclear Cr(VI)[6,8,9] dominates, although dichromium species have also been reported.[10,11] At higher chromium load, α-Cr_2O_3 particles start to appear.[8,11,12] The mononuclear Cr(VI) species have been characterized by IR and Raman spectroscopy to have distorted tetrahedral structure and to possess two doubly-bonded terminal oxo ligands.[6,9] In the reduction phase, both the nature of the surface, the reducing agent and the temperature influence the final composition. On silica, *CO* reduces Cr(VI) to Cr(II)[10,13] whereas H_2 and alkanes favors reduction to Cr(III).[13] Re-heating under humid conditions leads to re-oxidation of Cr(II) to Cr(III).[14–16]

There is some controversy concerning the oxidation state of chromium active for dehydrogenation of alkanes. Both Cr(II)[14,17] and Cr(III)[18–20] were proposed as the active state quite early on. The dominating view in the modern literature is that +III is the most active oxidation state for dehydrogenation, possibly with minor contributions from +II.[13,21–25]

Concerning the dispersion of active chromium, below mono-layer coverage and on both alumina, silica and zirconia, a linear relationship is found between the number of mononuclear Cr(VI)/Cr(V) species after calcination, and catalytic activity after reduction.[13,26–29] On this basis, DeRossi and co-workers[13,26,27] concluded that the reaction requires only mononuclear chromium species. This does not imply that CrOCr linkages are

**Correspondence to:* K. J. Børve, Department of Chemistry, University of Bergen, Allégaten 41, NO-5007 Bergen, Norway.
E-mail : knut.borve@kj.uib.no
†Paper presented at the 9th European Symposium on Organic Reactivity, 12–17 July 2003, Oslo, Norway.
Contract/grant sponsors: Research Council of Norway through the Programme for Supercomputing; Deutsche Forschungsgemeinschaft;
Contract/grant number: SFB 546.

detrimental,[13] polynuclear species are in fact reported to be highly active.[21,29,30]

In agreement with the cited observations, *redox* Cr(III) species, i.e. Cr(III) species resulting from reduction of Cr(VI)/Cr(V), have been identified as very likely being active for dehydrogenation.[13,22,23,27,31–33] On the other hand, in a recent contribution by Puurunen *et al.*[34] it was concluded that the activity of a Cr(III) ion is determined by its environment rather than its redox history.

On alumina, *in situ* diffuse-reflectance UV–vis spectroscopy (DRS) was used to establish a semi-quantitative relationship between the number of pseudooctahedral Cr(III) sites and dehydrogenation activity.[22] Infrared spectroscopy studies of *CO* and *NO* adsorbed onto reduced Cr species on silica[13] and zirconia[35] provide further clues. Together with measurements of dehydrogenation activity, these experiments lead to the conclusion that the most active Cr(III) has two coordinative vacancies. From its spectroscopic signature, this species was dubbed Cr(III)G, and DeRossi *et al.*[13] went on to propose a possible structure: chromium bonded to the surface through two oxygen bridges and with hydroxyl as the third ligand, cf. Fig. 1.

Only scattered information about the mechanism of dehydrogenation is available for chromium on alumina and none at all for silica. Starting with various ideas about the nature of the active site, a number of reaction mechanisms have been proposed, see Ref. 36 and references cited therein. A recurrent idea is that C—H activation could involve a Cr—O pair.[3,13,26,36,37] In agreement with the conclusions of DeRossi and coworkers concerning the activity of mononuclear chromium species,[13,26,27] Burwell *et al.*[37] and later Weckhuysen and Schoonheydt[3] proposed that dehydrogenation is initiated by physisorption of the alkane on coordinatively unsaturated Cr(III) centers. A C—H bond is subsequently activated and new O—H and Cr—alkyl bonds are being formed, cf. reaction (1) in Fig. 2. According to this mechanism, the alkene is formed as a result of hydrogen transfer from the alkyl to chromium, whereas regeneration of the catalytic site and formation of H_2 concludes the catalytic cycle, cf. reaction (3) in the figure.

At this point it appears fruitful to complement the many experimental studies of these systems by theoretical modeling of possible routes for dehydrogenation of ethane over Cr–oxide surface sites. In the present paper, we use gradient-corrected density functional theory in conjunction with cluster models of Cr(III)–silica surface

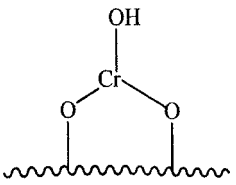

Figure 1. The Cr(III)G structure proposed in Ref. 13 to be active in dehydrogenation of alkanes

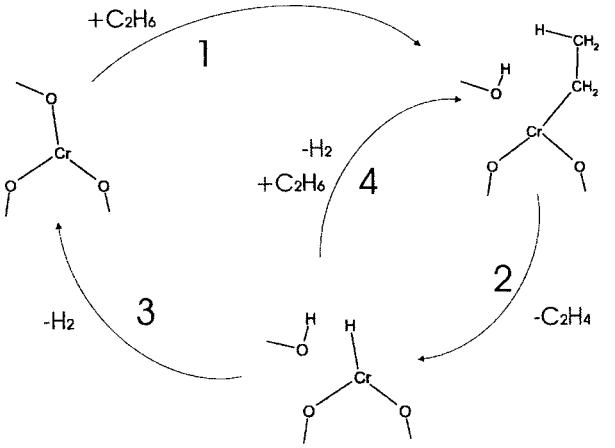

Figure 2. Schematic reaction mechanism for dehydrogenation of ethane over Cr–silica

sites to explore dehydrogenation of ethane. We focus on reaction mechanisms that largely follow the proposal by Weckhuysen and Schoonheydt[3] as outlined above, where C—H activation of the alkane takes place through direct interaction with chromium.

A number of mechanisms for C—H activation are known from organometallic chemistry, the two most relevant to the present system being oxidative and electrophilic addition, respectively.[38] During oxidative addition, both carbon and hydrogen bind directly to the metal as the C—H bond is broken. Electrophilic addition can also be described as a σ-bond metathesis reaction,[39] as a metal—ligand bond and a C—H bond are replaced by a metal—C bond and a ligand—H bond. Alternatively a metal—H and a ligand—C bond could be formed.[40,41] In general, σ-bond metathesis is favored on light electron-deficient metals, whereas oxidative addition is favored on the heavy and electron-rich late transition metals.[42–45] For chromium, σ-bond metathesis would be expected and is explored in this work. However, the possibility that dehydrogenation takes place by means of oxidative addition of the alkane can not be ruled out and will be investigated in subsequent work.

A major challenge in computational studies of any of the Cr–oxide systems is to develop realistic models of the chromium surface sites. We have extensive experience from modeling surface sites of Cr–silica in the context of ethylene polymerization and spectroscopy,[46] and also transition metal ions in siliceous structures.[47–51] In order to build on this, we chose silica as the initial substrate for our investigations of Cr–oxide catalysts for dehydrogenation, to be extended to the industrially more interesting Cr–alumina systems at a later stage. Taking the Cr(III)G structure proposed by DeRossi *et al.*[13] as our starting point, we have chosen to explore the more general, conceptual model of mononuclear Cr(III) with three covalent ligands that coordinate through oxygen. Cluster models are constructed either *ad hoc* by identifying likely coordination sites of chromium on low-index surfaces of

silicalite, or systematically by simulated annealing of chromium on low-index surfaces of low cristobalite. In order to validate the performance of the simple cluster models and to establish effects of an extended support, combined quantum mechanical–molecular mechanical (QM–MM) methods have been applied in conjunction with slab models.

The aim of the work is two-fold. Firstly, we want to explore whether the sequence of reaction steps suggested in Ref. 3 provides a viable route to alkane dehydrogenation on Cr(III) surface sites. Secondly, we aim to establish structural constraints on potentially active sites of dehydrogenation. This includes a study of how constraints imposed by the substrate influence the energy requirements of the various elementary steps during dehydrogenation.

MODELS

In this work, surface cluster models have been constructed either in an *ad hoc* manner, drawing on chemical intuition and what is known from experiment, or systematically, starting from low-index surfaces of silica crystals. With the *ad hoc* approach, specific characteristics of a surface site can be examined using relatively small and simple clusters, yet at the cost of neglecting potentially important surface effects. For instance, the essence of a Cr(III)G species as proposed by DeRossi *et al.*[13] is maintained in the hydroxychromium disiloxyether molecule shown in Fig. 3**A**, later referred to as the DeRossi-1 model. Here, chromium is bonded to two silicon atoms in the silica surface *via* two oxygen bridges, with the more distant parts of the silica being neglected and the dangling bonds terminated by hydrogen. The first coordination sphere of chromium is even reproduced by the $Cr(OH)_3$ molecule, see Fig. 3**B**, which defines a site completely void of surface constraints.

Improved models taking into account larger parts of the amorphous substrate can be generated from low index surfaces of the high-T modifications of silica; α- and β-cristobalite.[52–54] Molecular dynamics in conjunction with shell-model potentials are used to obtain structurally relaxed slab models of Cr-doped silica surfaces, see Plate 1 and e.g. Ref. 55 for a broader introduction. The steps of this procedure as applied here, are described in Computational Details.

Our approach is less than straightforward, in that the molecular dynamics simulation may take the system to structures outside the validity range of the shell-model potentials. As a result, artifacts such as three- and five-coordinated silicon atoms are frequent, as observed also by others.[56–59] Moreover, the potential used for H^+, used to neutralize the surface, is not optimal for describing hydrogen in silanol groups.[60] This implies that some amount of user intervention was required in order to generate realistic models, such as trying out different initial positions of the ions that were added to the surface and relocating O^{2-} or H^+ ions during the simulations. The final surface models that were used to study the dehydrogenation reaction, were chosen on the basis that a cluster region could be defined in which all silicon atoms were four-coordinated and there were no interstitial hydrogen atoms.

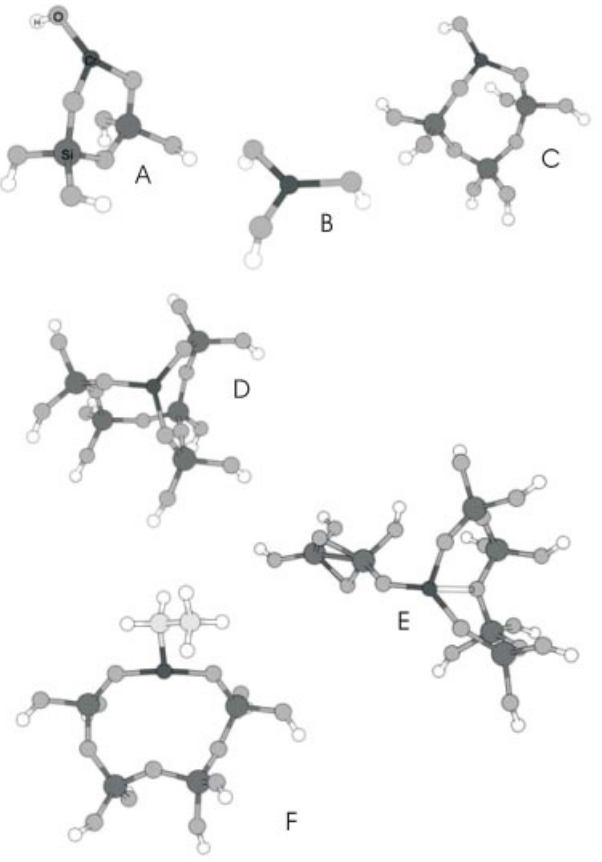

Figure 3. Cluster models of Cr(III)–silica surface sites: DeRossi-1 (**A**), $Cr(OH)_3$ (**B**), (100)-DeRossi (**C**), (101)-3bridge (**D**), (111)-3bridge (**E**) and mod-(111)-3bridge (**F**)

In each case, the cluster region includes chromium and its local chemical environment, with boundary bonds $O_{cluster}$—Si_{host} severed and terminating by hydrogen atoms. These clusters were used separate from the bulk in pure quantum mechanical (QM) cluster calculations, and as the QM region in QM–MM periodic boundary calculations. When used as isolated clusters, in resemblance of the restoring forces of the extended structures, atoms at the cluster boundaries have their positions fixed to those of the parent slab model. In the two-bridged models, this implies frozen positions for all atoms except those of the $(—O)_2$CrOH moiety. In the three-bridged models, the terminating $Si(OH)_n$ groups were held in fixed positions. The accuracy of this approach is examined in QM–MM optimization of slab models. An indication of the level of strain in each model is found by comparing the $(—O)_3$Cr geometry with that of the fully relaxed $Cr(OH)_3$, cf. Table 1. Apparently, the

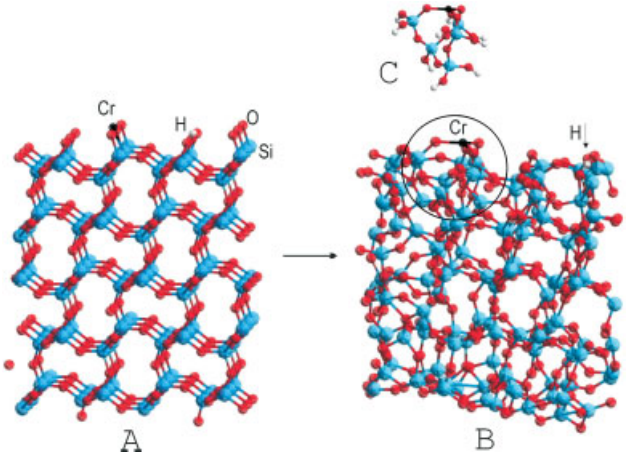

Plate 1. Systematic preparation of Cr–silica surface models using simulated annealing. A: The unrelaxed surface with Cr, H and O added B: The fully relaxed slab model following simulated annealing and optimization C: Cluster model with H-terminated dangling bonds

Table 1. Local geometry about chromium in the clusters

Cluster[a]	∠OCrO[b]	rCrO[b]
DeRossi-1	123.9, 123.9, 107.7	1.81, 1.81, 1.78
w-DeRossi-1	126.4, 126.4, 106.5	1.83, 1.83, 1.78
$Cr(OH)_3$	120.0	1.79
w-$Cr(OH)_3$	124.4, 112.0, 111.9	1.84, 1.84, 1.81
(100)-DeRossi	120.2, 119.7, 119.4	1.80, 1.80, 1.79
(101)-3bridge	130.3, 118.0, 110.4	1.83, 1.82, 1.77
(111)-3bridge	139.2, 113.1, 105.5	1.93, 1.92, 1.84

[a] Cluster labels are defined in Fig. 3, with a prefix (w) added to indicate the presence of preadsorbed water.
[b] Units: bond lengths (r) in Å, angle (∠) in degrees.

(100)- and (101)- based models are geometrically fairly relaxed, whereas the (111)-based Cr–silica model is more strained.

From the (100) surface of α-cristobalite, a DeRossi-type two-bridged Cr(III) species was generated, cf. Fig. 3**C**. This is later referred to as the (100)-DeRossi model. Simulated annealing was performed with a [1,2,5] super unit cell, with the cell parameter in the c-direction increased to 48.7 Å. To center the super unit cell about the cluster region, the super cell was further expanded to [2,4,5].

A three-bridged Cr(III) model was generated from the (101) surface and denoted by (101)-3bridge, cf. Fig. 3**D**. It was annealed using a [2,3,5] super unit cell, with a cell parameter in the c-direction of 36.4 Å.

A third systematic model was generated using a slab model of the (111) surface of α-cristobalite. The super unit cell was taken as [2,2,5], and the cell parameter in the c-direction was extended to 32.5 Å. The three-bridge chromium species results with chromium taking part in rings containing 4, 5 and 6 silicon atoms, respectively. In the cluster model, only the 6-ring is included, cf. Fig. 3**E**, and the model is referred to by (111)-3bridge. The (111)-3bridge site undergoes extensive relaxation when engaged in reactions, giving rise to the modified site mod-(111)- 3bridge shown in Fig. 3**F**.

At various points it will be instructive to consider these models with a precoordinated Lewis donor, for simplicity represented by a water molecule. The resulting models are denoted by the labels defined for each cluster, prefixed by w.

COMPUTATIONAL DETAILS

The quantum mechanical (QM) calculations have been performed using density functional theory as implemented in the Amsterdam Density Functional (ADF) set of programs.[61,62] For electron correlation the LDA functional of Vosko *et al.*[63] augmented by the nonlocal 1986 corrections by Perdew[64] were used. The exchange functional consisted of the Slater term augmented by gradient corrections as specified by Becke.[65]

Closed- and open-shell systems were described within spin-restricted and -unrestricted formalisms, respectively. The frozen-core approximation was used. Atomic cores were defined as the K-shell for first-row atoms and K- and L-shells for second- and third-row atoms. The number of basis functions used to describe the valence atomic orbitals were as follows: H 1s, 2; C 2s and 2p, 2; O 2s and 2p, 3; Si 3s and 3p, 2; Cr 3s and 3p, 2; Cr 3d and 4s, 3; and Cr 4p, 1. Polarization functions were added to all atoms but chromium. A single set of d-type polarization functions were added to C, O and Si, and a set of p functions were added to H. A set of auxiliary atom-centered s, p, d, f and g STO functions were used to fit the electron density as well as Coulomb and exchange potentials.

Molecular geometries were converged to a gradient below $0.001\,E_H\,(Å)^{-1}$ with the accuracy of the numerical integration schemes adjusted accordingly. The transition-state searches were typically conducted in two steps: a linear transit scan followed by transition-state optimization. The optimization was started from the highest point on the linear-transit energy curve, using a Hessian matrix calculated[66] at the B3LYP[67,68] level of theory in conjunction with 3-21G atomic bases.

In general, energy differences refer to electronic degrees of freedom only, i.e. without zero-point vibrational energies or temperature effects. For the dehydrogenation reaction, $C_2H_6 \rightarrow C_2H_4 + H_2$, the change in electronic energy is computed to $158\,kJ\,mol^{-1}$. However, in order to take into account temperature and entropy effects, the full set of thermodynamic functions were computed in the harmonic and rigid-rotor approximation for simulations based on the DeRossi-1 surface model. Maximal accuracy of the numerical integration schemes was used. All stationary structures display an ultrasoft vibrational mode that has been consistently omitted from the harmonic analysis. Tunneling corrections to the reaction barriers pertaining to hydrogen transfer has been estimated[69] and found to be negligible.

Molecular mechanics computations were performed using the General Utility Lattice Program (GULP).[70,71] The shell model was used, but with shells only on oxygen. H, Si, Cr(III) and Cr(II) were described as core only. The Si and O potentials were parameterized for silica structures by two of us.[60] The H potential was parameterized for link hydrogens in the QM-Pot QM–MM program.[60] Parameters for Cr(III) and Cr(II) are taken from Binks.[72]

Molecular dynamics in conjunction with shell-model potentials is used to obtain structurally relaxed slab models of Cr-doped silica surfaces, see Plate 1 and e.g. Ref. 55 for a broader introduction. The steps of the procedure as applied here, are as follows. (i) Slab models that expose low-index planes of crystalline low-cristobalite crystal are prepared by the Cerius program.[73] A super unit cell is defined to allow for relaxation at a larger length scale as detailed below. (ii) To generate chromium

species with three oxygen linkages to the surface, one Cr^{3+} ion is manually added per super unit cell in the vicinity of $(—O)_3Si—O^{-1}$ surface groups, with O^{2-} and H^+ ions added as needed to maintain neutrality. Similarly, Cr^{2+} was used to generate chromium species with two oxygen linkages to the surface. DeRossi-type Cr(III) species were formed by adding a hydroxyl ligand to the two-bridged chromium species. (iii) Each model is subjected to simulated annealing in terms of NVT dynamics,[59] i.e. the number of particles and the volume are kept constant while the energy is allowed to fluctuate in equilibrium with a thermostated bath. The process starts at 1500 K and the temperature is then lowered in steps of 150 K until 0 K is reached. At each temperature, NVT molecular dynamics is performed for 0.4 ps with time steps of 0.0005 ps. (iv) Finally, the structure is optimized under constant pressure conditions.

QM–MM geometry optimizations were performed using the QM-Pot mechanical embedding program of Sauer and Sierka.[74] In this implementation, the total energy to be minimized is given by Eqn (1).

$$E_{\text{total}} = E_{\text{host,MM}} - E_{\text{cluster,MM}} + E_{\text{cluster,QM}} \qquad (1)$$

The link atoms, i.e. the hydrogen atoms used to terminate the dangling covalent bonds of the cluster, were placed along the direction of the $O_{\text{cluster}}—Si_{\text{host}}$ bond as $O_{\text{cluster}}—H—Si_{\text{host}}$, at a fixed distance of 0.9666 Å from O_{cluster}. This is enforced during the QM–MM geometry optimization. As a result the gradients on the $O_{\text{cluster}}—Si_{\text{host}}$ bonds are due only to the host MM gradients.[75]

Shell-model potentials for the interaction between transition metals and hydrocarbon ligands are not easily constructed. In this work, ethane and fragments thereof have been omitted from the MM potential expression. Moreover, the long range electrostatic field from the region external to the cluster, is omitted from the QM Hamiltonian. Ideally, at the center of the cluster, gradient terms of the short-range MM potential cancel between the host and cluster regions. The gradients close to the center of the cluster are therefore mainly due to the cluster QM term and the host MM long-range electrostatic term, and for atoms originating from ethane, only QM gradient terms are taken into account.

To reduce the gradients as much as possible in the cluster region, the QM–MM optimizations were performed in the following sequence of steps. (i) The cluster geometry is optimized at the QM level of theory, with frozen coordinates of the boundary atoms. (ii) The full slab model is optimized at the QM–MM level of theory, until maximum and RMS gradients of the QM-Pot gradient become of the order of 10^{-2} and 10^{-3} E_H Å^{-1}, respectively, at which point numerical noise leads to oscillatory behavior. (iii) Atomic coordinates of substrate atoms external to the cluster were kept frozen except for silicon atoms neighboring the cluster, and the geometry was further refined until maximum and RMS gradients drop below 2×10^{-3} and $2 \times 10^{-4} E_H$ Å^{-1}, respectively.

RESULTS

Reactions on molecular cluster models of DeRossi-type sites

For simplicity, a chromium site will be referred to by the ligands in the first coordination sphere of the metal. For instance, a general DeRossi-type site is denoted by $(—O)_2CrOH$, where —O represents a generic oxygen ligand singly bonded to chromium. The reaction scheme of Fig. 2 is first presented and analyzed using the DeRossi-1 cluster model shown as Fig. 3**A**. For this model, the free energy profile of the catalytic reaction is computed and used to identify the rate-determining step. Subsequent models are then used to investigate the importance of the constraints imposed by the silica surface on the chromium site.

Reactions on the DeRossi-1 model. We have not been able to locate any molecular complexes between ethane and chromium on DeRossi-type Cr(III) sites. This implies that the initial encounter is reactive rather than physisorptive, contrary to the original proposal of Weckhuysen *et al.*[3] The initial reactive collision between the $(—O)_2CrOH$ site and ethane is henceforth assumed to follow a σ-bond metathesis mechanism, in which a C—H bond in ethane and the Cr—OH bond of the DeRossi site are broken and new ethyl—Cr and H—OH bonds are formed.

On the DeRossi-1 model, the concerted breaking of C—H and Cr—OH bonds and forming of ethyl—Cr and H—OH bonds proceeds in a single elementary reaction. The optimized structures of the stationary points of the reaction are shown in Fig. 4. The transition state of this first reaction step has a well-defined four-center character, where chromium assists the transfer of hydrogen from ethane to the hydroxyl oxygen. The electronic activation energy is computed to 138 kJ mol^{-1}, cf. Table 2, only slightly higher than the enthalpy of activation (135 kJ mol^{-1}). According to Table 2, the entropic contribution adds another 118 kJ mol^{-1} at 500 °C to the free energy of activation, mainly due to loss of translational degrees of freedom. The newly formed water molecule remains coordinated to the metal in the primary product, and the free energy of reaction is +178 kJ mol^{-1}. Changes in free energy and enthalpy along the catalytic cycle are shown graphically in Fig. 5, where the various reaction steps are numbered according to Fig. 4.

The second reaction step involves transfer of a hydrogen atom to chromium from the β-carbon, i.e. the methyl end of the ethyl ligand, accompanied by release of ethene, cf reaction **2** in Fig. 4. The reaction is found to

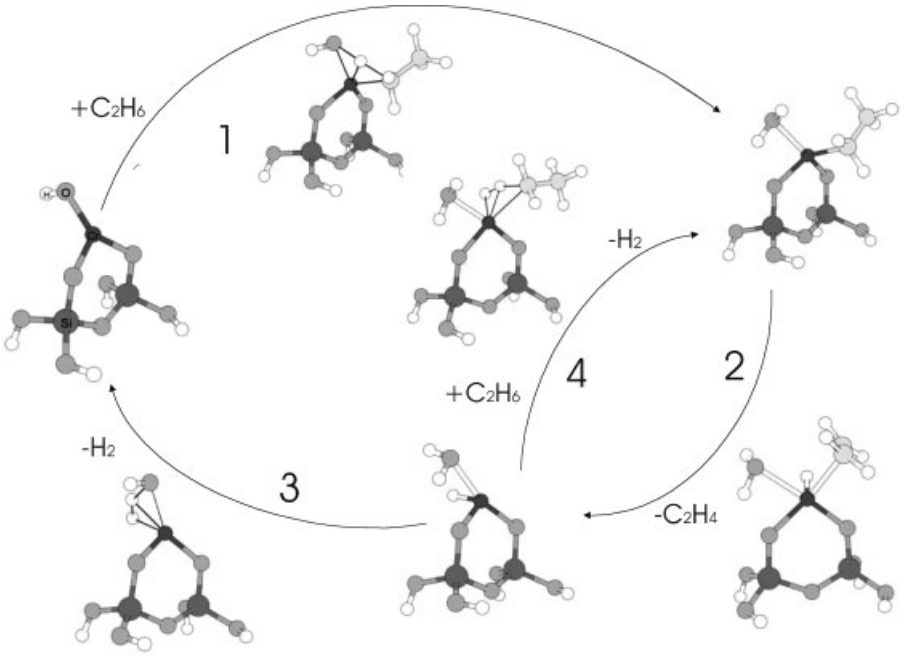

Figure 4. Optimized stationary structures for the dehydrogenation reaction of ethane over the DeRossi-1 model catalyst. The reaction steps are (**1**) C—H activation of ethane, (**2**) β-H transfer to chromium with subsequent loss of ethene, (**3**) Cr—O formation with subsequent loss of H_2 and (**4**) C—H activation of ethane with subsequent loss of H_2

proceed uphill in energy almost all the way to the primary product, in which ethene remains weakly bound. In terms of electronic energies, the transition state of this reaction step lies 79 kJ mol^{-1} above that of the reactant ethylchromium complex, and only 4 kJ mol^{-1} higher in energy than the product. At 500 °C the difference in enthalpy between transition state and product vanishes. This implies that decoordination of ethene is essential to prevent the hydrogen transfer reaction from running backwards. The coordination enthalpy of ethene is computed to be 37 kJ mol^{-1} cf. Table 2. However, there is an important entropic driving force for desorption of ethylene, amounting to -114 kJ mol^{-1} at 500 °C and decreasing with temperature. The net change in free energy of step (2) in Fig. 4 including release of ethene, thus becomes slightly negative, at -6 kJ mol^{-1}. The position of the activated complex is difficult to ascertain in this case, since it is given by the maximum in free energy which most likely occurs somewhere along the path of desorption of ethene. If the entropy increases significantly only after passing the transition state, the enthalpy of activation may be estimated to 100 kJ mol^{-1}, by adding the coordination energy of ethylene to the computed barrier of β-hydrogen transfer. This estimate is shown as a dotted line in Fig. 5. In order to quantify the amount by which the activation energy is lowered by entropic effects, variational transition state theory (VTST)[76] is needed, which is considered outside to be the scope of this work.

Once formed, the hydridochromium(III) complex is highly reactive and can react with surface oxygen species (XOH) under the release of molecular hydrogen, cf

Table 2. Thermodynamic functions (kJ mol^{-1}) at 500 °C and 1 atm of reactions (1–4) in Fig. 4 as computed for the DeRossi-1 cluster model. The water molecule produced in reaction (1) remains coordinated under reactions (2) and (4) and is consumed in reaction (3)

	Reaction (1)[a]		Reaction (2)[b]			Reaction (3)[c]		Reaction (4)[c]	
Parameter	TS	EthylCr $(OH_2)_{ads}$	TS	HydridoCr$(OH_2)_{ads}$ $(C_2H_4)_{ads}$	HydridoCr$(OH_2)_{ads}$ $+C_2H_4$ (g)	TS	$(—O)_3Cr$ $+H_2$ (g)	TS	EthylCr$(OH_2)_{ads}$ $+H_2$ (g)
ΔE_{elec}	138	66	79	75	124	62	−32	74	34
$\Delta E_{elec+ZPE}$	131	67	70	66	109	53	−52	71	15
ΔH	135	78	66	68	105	48	−59	74	26
$-T\Delta S$	118	100	22	3	−111	10	−95	127	5
ΔG	253	178	87	71	−6	58	−154	201	31

[a] Energies are given relative to separated $(—O)_3Cr$ model catalyst and ethane.
[b] Energies are given relative to the most stable conformation of the ethylchromium complex.
[c] Energies are given relative to the naked hydridochromium complex, i.e. after desorption of ethene.

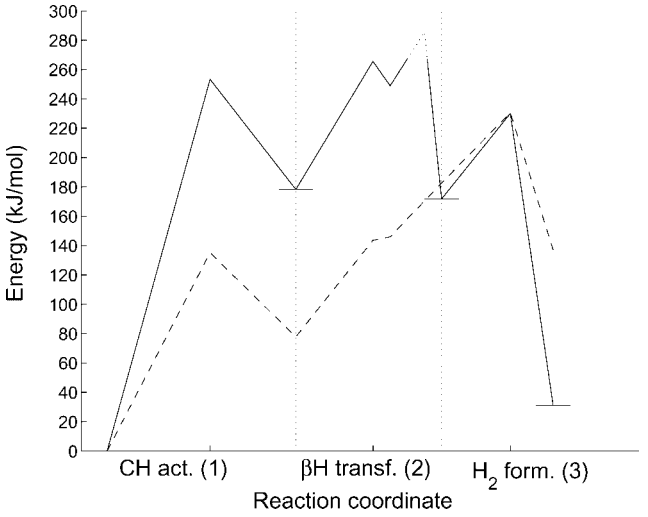

Figure 5. Free energy (full line) and enthalpy (dashed line) profiles of the (1,2,3) cycle shown in Fig. 4 for dehydrogenation of ethane over the DeRossi-1 model. A dotted line is used to represent the maximum free energy barrier of ethene desorption. Energies are given in kJ mol^{-1} relative to that of separated ethane and model catalyst. The reaction steps are: (1) C—H activation of ethane, (2) β-H transfer to chromium with subsequent loss of ethene, (3) Cr—O formation with subsequent loss of H_2

reaction (3) in Fig. 4. Potential reactants are water (X = H) or a vicinal surface silanol (X = Si). The reaction is energetically favorable, and in the case of a coordinated water molecule, shown at the lower left of Fig. 4, the enthalpy of reaction (3) is -58 kJ mol^{-1}. The activation enthalpy is computed to be 48 kJ mol^{-1}, which is low compared with reaction barriers for the two preceding steps.

From Fig. 5 it is evident that the second reaction step represents the highest point on the free-energy profile of the (1,2,3) cycle and it is therefore rate determining. If, as discussed above, the entropy increases significantly only after passing the transition state, the free energy of this point is approximately given by the free energy of the hydridochromium complex with ethene coordinated, plus the enthalpy of desorption. This implies that the overall kinetics of the catalytic cycle are determined by a free energy of activation of 286 kJ mol^{-1}, and an overall enthalpy of activation of 183 kJ mol^{-1}.

Alternatively, at a high pressure of ethane, the hydridochromium complex formed in reaction (2) by β-H transfer to the metal, can conceivably engage in a bimolecular σ-bond metathesis reaction with a second molecule of ethane. This leads to the release of molecular hydrogen, accompanied by the formation of an ethylchromium(III) complex. Stationary points for this elementary reaction is shown as reaction (4) in Fig. 4. The enthalpy of activation for this step is computed to be 74 kJ mol^{-1} at the hydridochromium DeRossi-1 site. The reaction enthalpy is 26 kJ mol^{-1}. Loss of translational freedom as ethane chemisorbs leads to a high free energy of activation of 201 kJ mol^{-1}. However, since H_2 shows no affinity toward chromium and is released to the gas-phase, the reaction is roughly isentropic.

At this point it seems that a bimolecular reaction between a short-lived hydridochromium species and ethane could form a viable route for C—H activation. In turn, an alternative reaction mechanism to the one shown in Fig. 2 could be postulated as a cyclic repetition of reactions (2) and (4) in Fig. 4. The free energy and enthalpy profiles of this cycle is shown in Fig. 6. The highest point on the free-energy profile is represented by reaction (4), chemisorption of ethane is thus rate-determining. The activation free energy and enthalpy are, respectively, 201 and 74 kJ mol^{-1}, which is considerably lower than those of the (1,2,3) cycle. In this perspective, reaction (1) describes activation of a dormant (—O)$_2$CrOH site and reaction (3) describes deactivation.

Dehydrogenation activity due to the alternative (4,2) cycle relies entirely on the population of hydridochromium complexes on the surface. As the free energy change of reaction (1) to form the ethylchromium complex is computed to 178 kJ mol^{-1}, the population appears to be small. However, for temperatures above 0 °C, the water molecule formed in reaction (1) is likely to desorb and to get flushed downstream. Under dry conditions, this means that the hydrido complex is stabilized for stoichiometric reasons, and the (4,2) cycle could become an important catalytic pathway of dehydrogenation, see Fig. 7. The activation enthalpy of this cycle is computed to 74 or 69 kJ mol^{-1}, depending on the presence or absence of a Lewis donor.

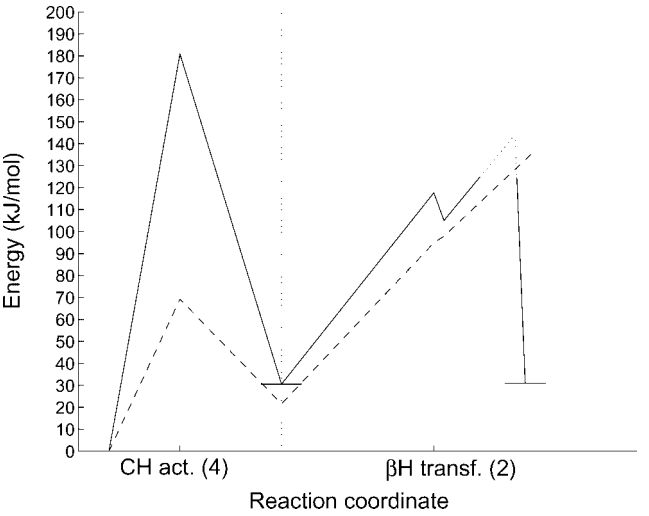

Figure 6. Free energy (full line) and enthalpy (dashed line) profiles of the (4,2) cycle shown in Fig. 7 for dehydrogenation of ethane over the DeRossi-1 hydridochromium model without a spectator water ligand present. A dotted line is used to represent the maximum free energy barrier of ethene desorption. Free energies are given in kJ mol^{-1} relative to that of separated ethane and the hydridochromium model catalyst. The reaction steps are (4) C—H activation of ethane with subsequent loss of H_2, and (2) β-H transfer to chromium with subsequent loss of ethene

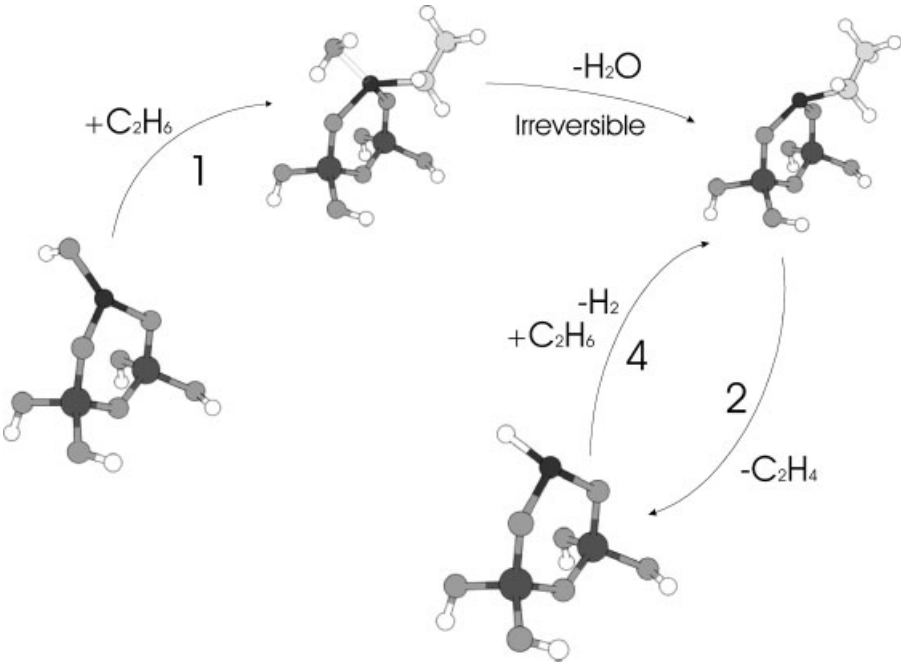

Figure 7. Optimized stationary structures for the dehydrogenation reaction of ethane over the DeRossi-1 model catalyst, assuming irreversible desorption of water. The reaction steps are (**1**) σ-bond metathesis C—H activation of ethane with subsequent loss of water, (**2**) β-H transfer to chromium with subsequent loss of ethene, (**4**) σ-bond metathesis C—H activation of ethane with subsequent loss of H_2

During the initial C—H activation step (1), the metathesis reaction may involve a Cr—O ester linkage to silica rather than the hydroxyl oxygen. This would lead to the formation of a surface silanol moiety instead of water. Relative to the energy of the unreacted cluster and free ethane, the electronic activation energy increases only by some $10\,kJ\,mol^{-1}$, cf. Tables 4 and 5, and Fig. 8. The silanol moiety coordinates only weakly to chromium, and the electronic energy barrier toward the subsequent β-hydrogen transfer is $78\,kJ\,mol^{-1}$, essentially the same as is discussed above. A notable difference, though, lies in that the silanol is likely to remain in the vicinity of chromium, yet less able than a water molecule to assume an optimal coordination to chromium. The energy of the ethyl- and hydridochromium complexes are elevated about $50\,kJ\,mol^{-1}$ compared with the case when water is formed in reaction (1), and coordinates to chromium. This could lend additional importance to reaction (3), i.e. regeneration of the chromium site with three covalent oxygen ligands, both due to increased collision frequency, a decrease in the activation energy by $45\,kJ\,mol^{-1}$, and a large and negative entropic contribution to the free energy associated with release of H_2 to the gas phase. Turning to the alternative (4,2) catalytic cycle, C—H activation according to reaction (4) at the hydridochromium(III)(siloxy)(hydroxy) complex is found to proceed with a modest electronic activation energy of $89\,kJ\,mol^{-1}$. However, taking into account the low activation energy found for reaction (3), the (4,2) cycle seems likely to be less important if the initial C—H activation involves hydrogen transfer to an oxygen linkage to silica.

Table 3. Thermodynamic functions ($kJ\,mol^{-1}$) at 500 °C for the desorption of water and reaction steps (2) and (4) in Fig. 4 as computed for the DeRossi-1 cluster model

	Desorption of water[a]	Reaction (2)[b]			Reaction (4)[c]	
Parameter	EthylCr $+ H_2O(g)$	TS	HydridoCr $(C_2H_4)_{ads}$	HydridoCr $+ C_2H_4$ (g)	TS	EthylCr $+ H_2(g)$
ΔE_{elec}	69	87	83	135	71	23
$\Delta E_{elec+ZPE}$	59	75	73	119	66	5
ΔH	57	73	76	115	69	15
$-T\Delta S$	−108	14	−2	−115	112	9
ΔG	−51	87	74	0	194	24

[a] Energies are given relative to the ethylchromium complex with water adsorbed.
[b] Energies are given relative to the most stable conformation of the ethylchromium complex.
[c] Energies are given relative to the naked hydridochromium complex, i.e. after desorption of ethene.

Table 4. Electronic energies (kJ mol^{-1}) of reactions (1–4) according to Fig. 4. The initial C—H activation takes place at the Cr—OH bond

	Reaction (1)[a]			Reaction (2)[b]			Reaction (3)[c]		Reaction (4)[c]	
Cluster model	TS	EthylCr $(OH_2)_{ads}$	EthylCr $+H_2O$ (g)	TS	HydridoCr $(C_2H_4)_{ads}$	HydridoCr $+C_2H_4$ (g)	TS	$(—O)_3Cr$ $+H_2$ (g)	TS	EthylCr $+H_2$ (g)
DeRossi-1[d]	138	66	—	79	75	124	62	−32	74	34
DeRossi-1	—	—	139	86	83	134	—	—	71	23
(100)-DeRossi[d]	139	67	—	106	98	122	61	−32	97	36
(100)-DeRossi	—	—	129	111	103	134	—	—	90	23
$Cr(OH)_3$[d]	150	83	—	92	85	113	58	−39	97	45
$Cr(OH)_3$	—	—	127	116	101	125	—	—	107	32
w-DeRossi-1	122	69	—	69	68	118	43	−31	51	39
w-$Cr(OH)_3$	127	73	—	87	82	109	49	−24	97	49

[a] Energies are given relative to separated $(—O)_3Cr$ model catalyst and ethane.
[b] Energies are given relative to the most stable conformation of the ethylchromium complex.
[c] Energies are given relative to the naked hydridochromium complex, i.e. after desorption of ethene.
[d] Water produced in reaction (1) remains coordinated under reactions (2) and (4) and is consumed in reaction (3).

The silica surface offers several types of oxygen species that could act as Lewis bases to chromium, including siloxanes, silanols and adsorbed water. To identify any qualitative effect such a donor could have on the dehydrogenation activity, a water molecule was coordinated to chromium prior to the initial C—H activation reaction (1). The labels of the resulting models are prefixed by w. In the w-DeRossi-1 model, the Cr—OH_2 bond length is 2.69 Å and water is bound by an electronic coordination energy of 50 kJ mol^{-1}. The Mulliken atomic charge on oxygen in the coordinated water molecule is initially $-0.53\,e$ and remains between -0.44 and $-0.47\,e$ throughout the catalytic reaction. This indicates that electrons are being donated to the $(—O)_2CrR$ moiety. In terms of energies, the transition states of reactions (1), (2) and (3) are all found to be slightly stabilized relative to the ethyl and hydridochromium complexes. This is also reflected in shorter Cr—OH_2 bonds in the transition states than in the unreacted clusters and reaction intermediates, indicating stronger dative bonds. Thus it appears that the presence of Lewis donors is likely to favor the dehydrogenation activity rather than retard it. However, given the fairly low coordination energy, only silanol groups are likely to maintain a stable presence, in which case the lack of structural flexibility is likely to limit any stabilizing effects on the reaction energy barriers.

Comparison between DeRossi-type models. As detailed under models, we have examined three realizations of the Cr(III)G type surface site: DeRossi-1, (100)-DeRossi and $Cr(OH)_3$, cf. Fig. 3. They differ in sophistication and ability to include constraints imposed by the surface. The generic reaction scheme described above has been explored and the results are summarized in terms of reaction energy profiles in Figs. 8 and 9 and in Table 4.

The simple $Cr(OH)_3$ model and the systematic (100)-DeRossi model give about the same electronic energy barrier for the C—H activation step (1) as already reported for DeRossi-1. There is a trend of decreasing coordination energy of the water molecule formed with increasing O—Cr—O angle. This makes desorption of water even more likely on the (100)-DeRossi model and hence on DeRossi-type surface sites than discussed above.

Turning to β-hydrogen transfer (2), the electronic energy barrier is computed to 111 and 116 kJ mol^{-1} on the (100)-DeRossi and $Cr(OH)_3$ models, respectively, to be compared with 86 kJ mol^{-1} on the DeRossi-1 model. However, these barriers reflect the coordination energy of ethene. Since loss of ethene is a prerequisite to stabilize the product, it is more instructive to compare the sum of the electronic activation energy and the energy of desorbing

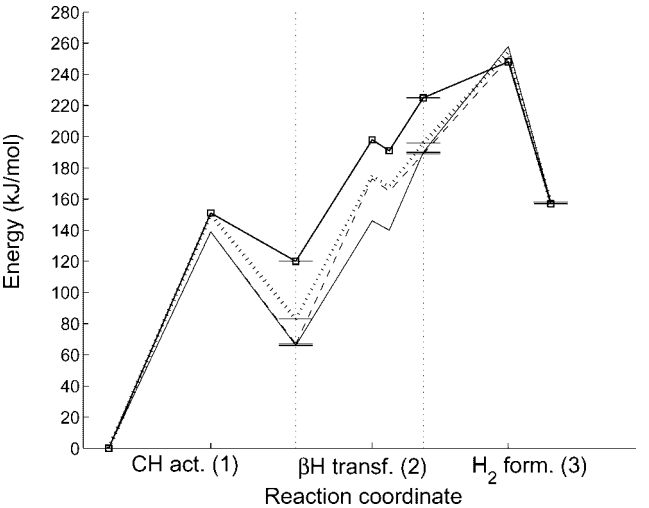

Figure 8. Electronic energy profile of the full catalytic cycle (1,2,3) shown in Fig. 4. Hydrogen is transferred to the Cr—O ester oxygen of the DeRossi-1 model (full line with square markers), and to the hydroxyl group of the DeRossi-1 (full line), (100)-DeRossi (dashed) and $Cr(OH)_3$ (dotted) models. The energies are given in kJ mol^{-1} relative to that of separated ethane and the model catalyst. The reaction steps are (1) C—H activation of ethane, (2) β-H transfer to chromium with subsequent loss of ethene, (3) Cr—O formation with subsequent loss of H_2

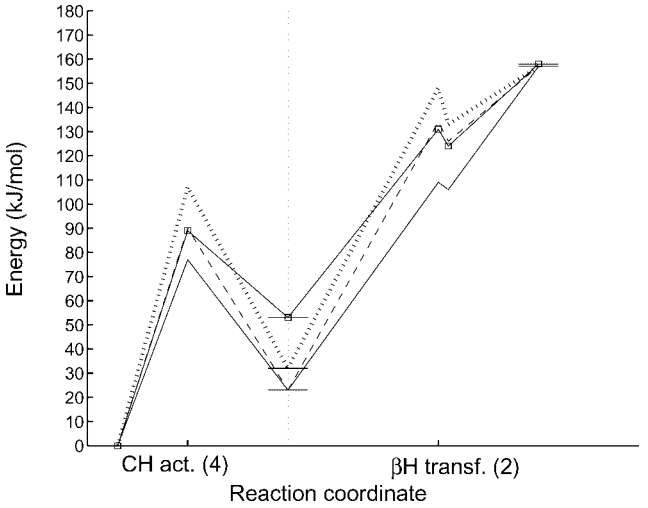

Figure 9. Electronic energy profile of the catalytic cycle (4,2) shown in Fig. 4 and Fig. 7 for dehydrogenation of ethane over the DeRossi-1 (full line), (100)-DeRossi (dashed) and $Cr(OH)_3$ (dotted) models without a spectator water, and over the DeRossi-1 model with a silanol coordinating to chromium (full line with square markers). The reaction steps are (4) C—H activation of ethane with subsequent loss of H_2, and (2) β-H transfer to chromium with subsequent loss of ethene. The energies are given in kJ mol^{-1} relative to that of separated ethane and hydridochromium model catalyst

ethene. The resulting values are 134 kJ mol^{-1} on DeRossi-1 and (100)-DeRossi, and 125 kJ mol^{-1} on $Cr(OH)_3$. For reaction (3), both activation energies and reaction energies agree between the three models, cf. the entries in Table 4 that are superscripted by *d*.

Somewhat larger differences between the models were computed for C—H activation of ethane over the hydridochromium complexes according to reaction (4) in Fig. 4. The electronic energy barriers were obtained as 71, 90 and 107 kJ mol^{-1} respectively on the DeRossi-1, (100)-DeRossi and $Cr(OH)_3$ models without any spectator water. The barrier decreases with increase in the angular strain in the linkage of chromium to the substrate. For the hydridochromium complex of the DeRossi-1, (100)-DeRossi and $Cr(OH)_3$ clusters, $\angle$OCrO assumes values of 111°, 124° and 131°, respectively, to be compared with the corresponding values at the transitions states, of 105°, 115° and 105°. Since the $Cr(OH)_3$ model displays completely relaxed bond angles, it is evident that the decrease in reaction barrier with narrower $\angle$OCrO is due to destabilization of the reactant rather than stabilization of the transition state.

Reactions over three-bridged Cr(III) surface sites

A second class of chromium surface sites related to the DeRossi-type of sites is obtained by allowing three oxygen atoms, rather than two, to form ester likages between chromium and the silica surface. This class of chromium species will be referred to as three-bridged species. We have studied the same reaction mechanisms as for the DeRossi-type models. A novel feature is that during the initial C—H activation, reaction (1) in Fig. 10 and Fig. 12, a surface silanol rather than water is formed. Depending on the strain in the Cr—O bond that is

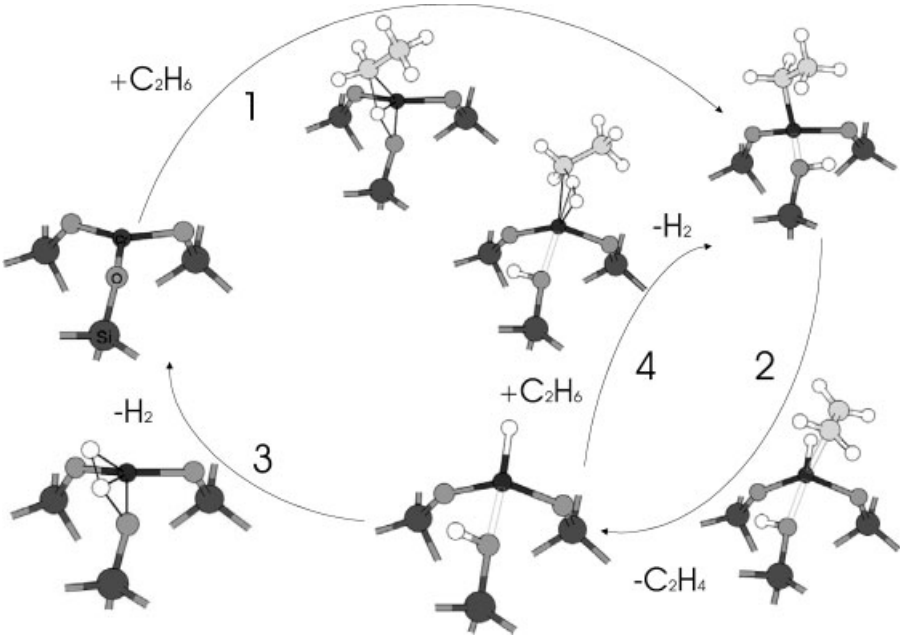

Figure 10. Optimized stationary structures for the dehydrogenation reaction of ethane over the (101)-3bridge model catalyst. The reaction steps are (**1**) σ-bond metathesis C—H activation of ethane, (**2**) β—H transfer to chromium with subsequent loss of ethene, (**3**) σ-bond metathesis O—H activation with subsequent loss of H_2, and (**4**) σ-bond metathesis C—H activation of ethane with subsequent loss of H_2

Table 5. Electronic energies (kJ mol^{-1}) of reactions (1–4) according to Fig. 10. The initial C—H activation takes place at a Cr—OSi bond

	Reaction (1)[a]		Reaction (2)[b]			Reaction (3)[c]		Reaction (4)[c]	
Cluster model	TS	EthylCr + —SiOH	TS	HydridoCr $(C_2H_4)_{ads}$	HydridoCr + C_2H_4 (g)	TS	(—O)$_3$Cr + H_2 (g)	TS	EthylCr + H_2 (g)
DeRossi-1	151	120	78	71	105	23	− 58	89	53
(101)-3bridge	161	109[d], 114, 120	100	108	136, 137	33	− 89	67	21
(101)-3bridge[e]	—	90[d], 86, 102	—	—	153, 141	—	—	—	—
(111)-3bridge	80	42, 45							
Mod-(111)-3bridge	—	—[d]	103	102	137	—	—	85	21

[a] Energies are given relative to separated (− O)$_3$Cr model catalyst and ethane.
[b] Energies are given relative to the most stable conformation of the ethylchromium complex, except when indicated[e].
[c] Energies are given relative to the naked hydridochromium complex, i.e. after desorption of ethene.
[d] Reference conformation of the ethylchromium complex.
[e] QM/MM results for the (101)-3bridge cluster embedded in mechanical slab model.

broken, the silanol group can remain close to or relax away from chromium.

Three-bridged surface site on the (101) surface of cristobalite. Our results are first presented for the (101) model of Fig. 3**D**. Energies are summarized in Table 5. The energy profile of the (1,2,3) cycle is shown in Fig. 11 as obtained for the (101)-3bridge site as well as the DeRossi-1 model with the initial C—H activation step involving a Cr—O ester linkage.

Activation of the three-bridged site according to (1) in Fig. 10 takes place with a reaction barrier of 161 kJ mol^{-1}. The thus formed ethylchromium complex has three stable conformations at energies of 109 to 120 kJ mol^{-1} above that of the reactants. The energetics of this reaction is similar to that computed for the DeRossi-1 model when hydrogen is transferred to a Cr—O ester linkage instead of to the hydroxyl ligand. In two out of three conformations, the ethyl moiety assumes a staggared conformation and the conformations differ mainly with respect to how strongly the silanol is coordinated to chromium. This is evident from Cr—O(silanol) distances of 2.06 and 2.50 Å, respectively. In the third conformation, the ethyl ligand forms a secondary β-agostic bond to the metal, and the r(Cr—O) distance is 2.12 Å.

The transition state of the subsequent β-hydrogen transfer, reaction (2), is 100 kJ mol^{-1} higher in energy than that of the most stable of the ethylchromium conformations. As for the DeRossi models, the transfer reaction is instantly reversed unless ethene desorbs to the gas phase. Moreover, in this particular case, the optimized hydridochromium complex with weakly coordinating ethene is slightly higher in energy than the transiton state of the β-hydrogen transfer, probably due to minor conformational changes.

Addition of the decoordination energy of ethene places the top point of the electronic energy profile of reaction (2) in Fig. 10 at 136 kJ mol^{-1}, about the same as for the DeRossi models. The thus formed hydridochromium complex displays a conformational equilibrium similar to what was described for the ethyl complex. The presence of conformations with long Cr—silanol distances could act to decrease the rate of deactivation of the hydridochromium complex according to reaction (3) as a result of decreased collision frequency. If the hydridochromium complex lives sufficiently long, it could react with ethane in a bimolecular σ-bond metathesis step, to release molecular hydrogen to the gas phase and to produce an ethylchromium site according to reaction (4) in Fig. 10. The electronic energy barrier to C—H activation is a low 67 kJ mol^{-1} and the electronic energy of the reaction is 21 kJ mol^{-1}, both numbers computed relative to the reactants of reaction (4). However, the

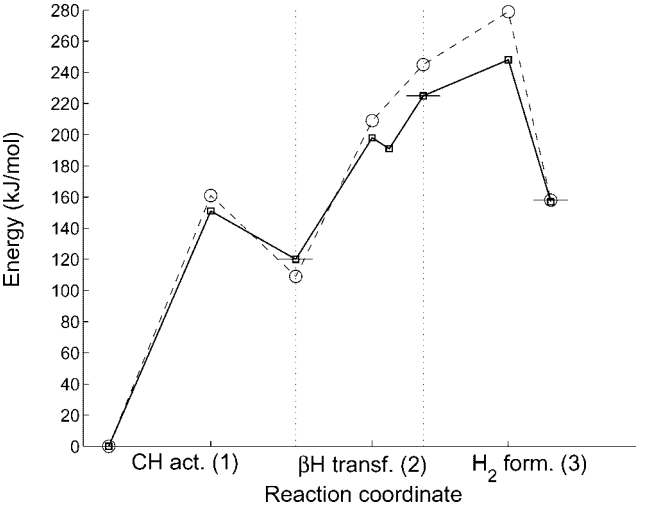

Figure 11. Electronic energy profile of the full catalytic cycle (1,2,3) shown in Figs. 4 and 10 for dehydrogenation of ethane. In the C—H activation hydrogen is transferred to a Cr—OSi linkage. The plots correspond to the DeRossi-1 model (full line with square markers) and (101)-3bridge model (dashed, open circles). The energies are given in kJ mol^{-1} relative to that of separated ethane and the model catalyst. The reaction steps are (1) C—H activation of ethane, (2) β-H transfer to chromium with subsequent loss of ethene, (3) Cr—O formation with subsequent loss of H_2

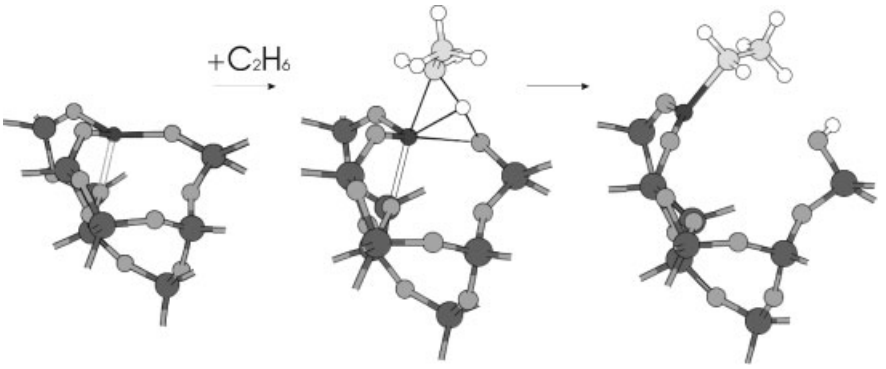

Figure 12. C—H activation by σ-bond metathesis, reaction (1), on the (111)-3bridge model catalyst. A silanol group is formed, and optimization at the QM–MM level of theory makes the Cr—silanol distance increase to more than 5 Å as the surface relaxes. The unreacted chromium site is optimized at the QM-MM level, and the transition state of C—H activation is optimized at the cluster QM level. For details concerning optimization of the ethyl complex, see the text

electronic barrier of the unimolecular reaction (3) involving the silanol moiety formed in (1) is even lower, at a mere 33 kJ mol^{-1}, cf. Table 5. The (101)-3bridge site is then reproduced in a strongly exothermic reaction both in terms of electronic energy and even more so in terms of free energy.

Results presented thus far were based on cluster models in which positions of the outer Si(OH)$_n$ groups were frozen. Clearly, the rigidity of this model is exaggerated. To improve our model, we include a mechanical embedding of the cluster, thus allowing for relaxation of the surface through optimization of all atomic positions. Some relaxation of the substrate is found to take place, in particular when forming the chromiumethyl site according to reaction (1). Here, surface relaxation stabilizes the product by about 20 kJ mol^{-1} relative to the reactants. Importantly, the structures and relative energies of the different conformations change only little, cf. Table 5.

Three-bridged surface site on the (111) surface of cristobalite. Starting from the (111)-surface of cristobalite, we prepared a three-bridged Cr(III) surface site that is considerably more strained than what was found for the (101) surface, cf. under Models. Noteworthy features of this model are that chromium is stabilized by donation from a siloxane moiety from beneath the surface, and that one of the silicon atoms linked to chromium, also takes part in a two-membered ring, see Fig. 3**E**.

Unlike the (101)-model, inclusion of mechanical embedding leads to results that are qualitatively different from those obtained for the naked cluster. For instance, starting from the cluster-optimized structure of the product of reaction (1), i.e. an ethylchromium complex with a nearby surface silanol, optimization at the QM–MM level of theory makes the Cr-silanol distance increase to more than 5 Å as the surface relaxes, see Fig. 13. The optimization then breaks down as the double siloxane bridge is ruptured in favor of single siloxane bridges, leaving the cluster termination invalid. Evidently, at strained surface sites such as modelled here, chemical activation of bonds linking chromium to the substrate can lead to irreversible surface relaxation.

In order to estimate reaction barriers, we have used several cluster models, each based on reactant structures that have been relaxed at the QM–MM level of theory. These models are likely to provide an upper estimate of the activation energies. For reaction (1) in Fig. 12, the barrier to C—H activation is found to be 80 kJ mol^{-1}. This number can be compared with 161 kJ mol^{-1} for the (101) three-bridge site, and 120–150 kJ mol^{-1} for various DeRossi-type sites, and it is apparently very low. A possible reason could be extra stabilization of the transition state by the sub-surface siloxane coordinating to chromium. This hypothesis was explored using a cluster model in which the coordinating siloxane was removed, see Fig. 3**F**. The activation energy increases to 100 kJ mol^{-1} on this modified model, which points to a stabilization of the transition state by 20 kJ mol^{-1}, similar to what was found for Lewis donors on DeRossi-type sites. The low activation energy of the initial σ-bond metathesis step is therefore mainly ascribed to the strained geometry of the reactant chromium site.

As the Cr—O bond is broken, the thus-formed silanol group relaxes into a position removed from Cr, see Fig. 12. The remaining ethylchromium surface complex resembles that of DeRossi-type models after desorption of water. To study subsequent steps in the reaction cycle, a new cluster model was defined from the QM–MM-relaxed structure, see Fig. 3**F**. The remote silanol group is not included.

Relative to the ethylchromium complex of the modified cluster model, the electronic energy barrier of the β-hydrogen transfer step (2) is computed to 103 kJ mol^{-1}. Throughout the reaction, the sub-surface siloxane donor has a dynamic behavior and assumes a position farthest to chromium at the transition state. Again, there is only a very shallow minimum for the hydridochromium complex as long as ethene remains coordinated, and a better

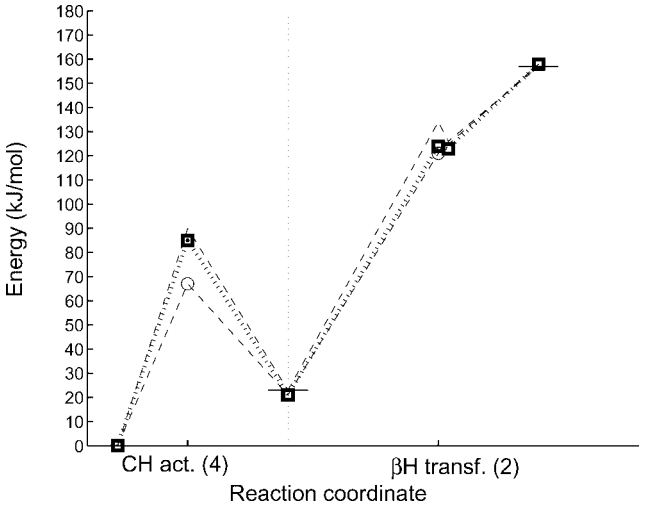

Figure 13. Electronic energy profile of the catalytic cycle (4,2) shown in Figs. 4, 7 and 10 for dehydrogenation of ethane over the (100)-DeRossi model without a spectator water (dashed), the (101)-3bridge model (dashed, open circles) and the mod- (111)-3bridge model (dotted, squares). The reaction steps are (4) C—H activation of ethane with subsequent loss of H_2 and (2) β-H transfer to chromium with subsequent loss of ethene. The energies are given in kJ mol^{-1} relative to that of separated ethane and hydridochromium model catalyst

measure of the energy requirement of this step is obtained by adding the decoordination energy of ethene ($\approx$40 kJ mol^{-1}) to the electronic energy barrier. The energy barrier toward C—H activation at the hydridochromium complex is computed to 85 kJ mol^{-1} relative to the energies of the reactants. Thus, apart from the ease with which the initial C—H activation reaction (1) takes place, the energy changes associated with dehydrogenation at the (111)-3bridge site are similar to those associated with the more relaxed (101)-3bridge and (100)-DeRossi models, cf. Fig. 13.

DISCUSSION

The aim of this work is to obtain an understanding of the relationship between the structure of Cr–silica surface sites and their ability to dehydrogenate ethane. Since our results rely on the validity of the adopted models of Cr–silica surface species, the models are first discussed on the basis of what is known from other studies of amorphous silica in general and the Cr-silica surface in particular.

We have applied both *ad hoc* cluster models and cluster and slab models based on the cristobalite structure. The simpler models have been validated by comparison with slab models for reactant and product structures, but not for transition states. At the transition state of reaction (1), i.e. C—H activation according to σ-bond metathesis, the Cr—O distances are close to their equilibrium values and little relaxation is expected on the silica part. This means that the forward barrier of this reaction step is expected to be fairly insensitive to surface relaxation, whereas the barrier to reforging a Cr—OSi bond could be underestimated by 10–20 kJ mol^{-1}. For elementary steps not involving breaking of oxygen bridges, i.e. β-hydrogen transfer and C—H activation at the hydridochromium species, surface and bulk relaxation is small.

Gibbs free energies have been computed only for reactions on the DeRossi-1 model and used to locate the rate-determining steps. For the other models, comparisons have been made on the basis of electronic energies. Entropic and temperature contributions to free energies are dominated by translational and rotational contributions, which are independent of the surface model. When comparing different surface sites, the differential contribution from zero-point vibrational energies is expected to be small relative to the differences in electronic energies.

The use of cristobalite to model amorphous silica is well precedented.[52–54,77] This structure consists of six-membered rings of silicon tetrahedra. Following simulated annealing, the six-membered rings still dominate in the bulk, although there are some occurrences of three-membered rings. The surfaces consist of six-, four-, three- and even two-membered rings, counting only the silicon atoms. The existence of two-membered rings on amorphous silica surfaces is controversial but also observed in other simulation studies.[53,54,78,79] It has been suggested that the absorption at 450 cm^{-1} observed in the Raman spectrum of vitreous silica could be due to two-membered rings.[53,78] Two-membered rings are also claimed to have been observed by ^{29}Si NMR.[80,81] Bulk amorphous silica shows no long-range regularity,[82] in contrast to our slab models, which show translational symmetry by way of construction. Owing to the localized character of the chemical interaction, we do not believe that this is an important limitation in the applied models.

As outlined in the Introduction, chromium is believed to be anchored to the silica surface through one or more oxygen bridges, formed in a reaction with surface silanols.[5–7] Hakuli *et al.*[24] observed a decrease in the number of isolated silanol groups during the calcination step of catalyst preparation. This might indicate that the chromium precursor reacts with isolated silanol groups. Alternatively, under wet conditions vicinal silanol groups could be formed through hydration of surface Si—O bonds.[54,83] Two-membered rings are the more reactive,[54] and hydration followed by anchoring of chromium would result in surface species similar to that of the DeRossi-1 and model, cf. Fig. 3. The analogous reaction sequence on a three-membered ring would lead to a two-bridged chromium species similar to that of the (101)-DeRossi model.

On defects of crystalline silicalite, most notably those missing silicon atoms, nests of hydroxyl groups are formed.[84] With several silanol groups in close vicinity, formation of triply-bridged chromium species becomes a distinct possibility, corresponding to our (101)-3bridge

model. Strained three-bridged species as in the (111)-3bridge model, are less likely for enthalpic reasons, as they would be unstable toward surface reorganization. On the other hand, it is a well-known aspect of catalysis that minority species associated with defects could be responsible for the observed activity.

Reports on the mechanism of dehydrogenation of alkanes over Cr–oxide catalysts pertain mainly to alumina, and no reports have been found for the case of silica. However, differences in activity as observed between the various substrates are often discussed in view of their capability to stabilize similar active species[25] rather than to open radically different reaction paths. We are presently extending our work to the Cr–alumina system, which in time will allow us to address this conjecture. At present, we will discuss our results on the background of observations made for different Cr–oxide systems, most notably Cr–alumina.

DeRossi *et al.*[13,26,27] concluded that only mononuclear chromium species are required for the reaction. On this basis we have studied the mechanism put forth by Burwell *et al.*[37] and Weckhuysen and Schoonheydt.[3] The proposal involves the following four steps: (0) physisorption of ethane on coordinatively unsaturated Cr(III)-centers; (1) activation of a C—H bond, accompanied by formation of O—H and Cr—C bonds; (2) alkene formation through β-hydrogen transfer; (3) regeneration of the catalytic surface through the formation of H_2. Apart from the initial physisorption of ethane on Cr, this mechanism amounts to steps 1–3 in Fig. 2.

Our calculations show that the coordination energy of ethane to chromium is negligible, and that the same applies to H_2. Even at the more polar alumina surface, taking into account the elevated temperatures at which the reaction takes place, it appears that adsorption would require a reactive collision of ethane on the chromium site, making the C—H activation step follow Eley–Rideal kinetics. With this modification, our results show that a cycle consisting of the three last steps does indeed constitute a viable mechanism.

C—H activation is energetically costly with a reaction barrier in the range 120–160 kJ mol^{-1}. Unless surface strain acts to weaken the Cr—O bond, the strengths of the involved bonds are such that the reaction becomes highly endothermic. Furthermore, at high temperatures, surface-catalyzed reactions are partially driven by increase in entropy upon desorption of product molecules. The (1,2,3) cycle involves two elementary reactions before ethene desorbs as the first product molecule. The free energy increases until this happens, which makes reaction (2) rate determining. The overall free energy and enthalpy of activation are correspondingly relatively high.

The activation free energy of the (1,2,3) cycle as computed for the DeRossi-1 model and C—H activation involving the hydroxyl ligand, is computed in the range 266–286 kJ mol^{-1}, depending on the point at which the entropy increases associated with desorption of ethene start to outweigh the losses in coordination energy. However, the water formed in reaction (1) on DeRossi species is likely to desorb, thus preventing regeneration of the chromium species. Activity due to the (1,2,3) cycle is therefore more likely to involve Cr—O ester linkages to the surface, with formation of a silanol moiety during the initial C—H activation step. In this case, weak coordination of silanol to the metal results in a higher electronic energy of the ethyl complex and consequently also of the rate-determining step of the cycle, which involves β-hydrogen transfer and ethene desorption. The increase in energy amounts to about 50 kJ mol^{-1}, which appears also in the overall enthalpy and free energy of activation. The lowest values of activation enthalpy and free energy of the (1,2,3) cycle are thus in the order of 200 and 300 kJ mol^{-1}, respectively. This gives a reaction rate constant in the order of 5.5×10^{-9} mol^{-1} m^3 s^{-1} per (—O)$_3$Cr species at 500 °C.

An alternative mechanism is apparent from our calculations, in which H_2 formation and C—H activation take place in a second, concerted reaction between chromium and ethane. Since C—H activation takes place at the reactive hydride complex rather than at a fairly stable chromium species with three oxygen ligands, the activation barrier for C—H activation becomes markedly lower. Still, the entropy loss associated with chemisorption of ethane contributes to make C—H activation the rate determining step for the (4,2) cycle. On the DeRossi-1 model and in the absence of a spectator water ligand, the activation free energy of the (4,2) cycle is 181 kJ mol^{-1}, corresponding to a rate constant at 500 °C of 0.6 mol^{-1} m^3 s^{-1} per hydridochromium complex. The second of the two steps in this mechanism is β-hydrogen transfer to the metal, to form ethene and to regenerate the hydride. The same reaction step in reverse has previously been proposed for the initiation phase during Phillips polymerization.[85] Considering the similarity of the preparation of these systems it is not unlikely that the same elementary step is present in both reactions, with the direction governed by the stoichiometry of the feed.

Using propane pressure of 5 kN m^{-2} in flow experiments at 500 °C, a turnover frequency in the order of 10^{-3} molecules s^{-1} per surface Cr atom was observed on Cr–silica.[13] On the basis of our computed free energies of activation, turnover frequencies in the order of 10^{-1} molecules s^{-1} per hydridochromium complex are obtained for the (4,2) cycle and 10^{-9} molecules s^{-1} per (—O)$_3$Cr species for the (1,2,3) cycle.

Converting to overall activation enthalpies, we have found the activation energy to be in excess of 200 and 70 kJ mol^{-1}, respectively for the (1,2,3) and (4,2) cycles. For comparison, activation energies of 88 ± 10 kJ mol^{-1} on Cr–silica, 67 ± 10 kJ mol^{-1} on Cr–alumina, 76 ± 10 kJ mol^{-1} on α-chromia have been reported for the dehydrogenation of propane.[13] All are comparable to that of the (4,2) cycle. However, an activation energy of

about 140 kJ mol^{-1} is reported for dehydrogenation of isobutane on Cr–alumina.[86]

The mechanism of C—H activation is a crucial question in the dehydrogenation mechanism. Several workers have proposed C—H activation to involve a Cr—O pair.[3,13,26,36,37] An indication that this could be the case is that hydridochromium and surface hydroxy groups were detected by IR upon dosage of hydrogen over chromia.[87] In another study, the Cr–zirconia catalyst has been found to be poisoned by K^+, possibly due to coordination to oxygen atoms near Cr to the extent that C—H activation is prevented.[88] On the Cr–alumina system, rearrangement of the surface is observed upon exposure to dehydrogenation conditions.[13] This could indicate irreversible loss of Cr—O bonds, preventing reaction (3) in Figs. 2 and 10. Puurunen *et al.*[34] performed dehydrogenation experiments with chromium deposited on alumina surfaced by aluminum nitride. While the replacement of oxygen by the more basic nitrogen was expected to increase the probability of dissociation of the alkane, and thereby the rate of dehydrogenation, the opposite was found. These workers concluded that nearby oxygen may be required to obtain chromium sites with high activity. An alternative explanation could be that in the dominant catalytic cycle of elementary reactions, C—H activation does not involve a structural anionic ligand, but rather a hydride. In this case the vicinity to chromium of the ligand—H group formed in reaction (1) will determine the activity as the hydride is easily consumed in reaction (3) unless the ligand—H group is removed from chromium. In turn, this may lend support to the (4,2) cycle.

In kinetic modeling of the dehydrogenation reaction of isobutane on Cr–alumina, it was found that adsorption parameters of both isobutane and H_2 had to be included to describe the reaction rate satisfactorily.[36] It was proposed that adsorption might include a Cr—O pair, as shown in steps (1) and (3) of Figs. 2 and 10. Moreover, adsorption of the alkane was found to be rate determining. In our computations the surface reaction (2) of β-hydrogen transfer appears rate-determining for the (1,2,3) cycle. This could suggest that on the more polar alumina surface, the hydridochromium(ethene) species is considerably stabilized as compared with Cr–silica. Alternatively, activity is largely due to the (4,2) cycle, of which C—H activation is found to be rate determining. Although activation at a hydridochromium complex was not considered in the study of Airaksinen *et al.*,[36] the necessity to include adsorption parameters of both isobutane and H_2 to describe satisfactorily the reaction rate, is consistent with the reversibility of reaction (4), C—H activation at a hydridochromium complex.

Prevention of reaction (3), reforging of the Cr—O bond, is a prerequisite for anything but sporadic activity of the (4,2) cycle and appears to be very sensitive to the local surrounding of chromium. DeRossi-type species are favorable in the sense that any water molecule formed in the initial C—H/Cr—O activation step, is likely to desorb and thereby render regeneration of the Cr—OH bond and thus termination of the (4,2) cycle unlikely, see Fig. 7. On the three-bridged surface species, a silanol group is made in the initial C—H/Cr—O activation. Depending on the geometric constraints on the chromium site, reformation of the Cr—O bond could be facile or difficult. For a fairly relaxed surface species, the silanol group is likely to stay coordinated to chromium. The average number of turns of the (4,2) cycle before deactivation according to reaction (3) is probably higher for strained (—O)$_3$Cr species where the silanol group relaxes away from chromium, see Fig. 12.

Small amounts of water on the surface have been found to be detrimental to the dehydrogenation activity.[88] This has been ascribed to competing coordination on chromium or rearrangement of the surface following hydration of oxygen bridges linking chromium to the surface.[86] The observation is also consistent with the (4,2) cycle of Fig. 4 being more active than the (1,2,3) cycle, since addition of water would remove any hydridochromium sites. Since both hydrogen atoms are predicted to originate from the same ethane according to the (1,2,3) cycle and from two different ethane molecules in the (4,2) cycle, these mechanisms can be distinguished in isotopic labeling experiments.

CONCLUSIONS

Mechanistic aspects of dehydrogenation of ethane over mononuclear Cr(III)–silica have been studied by means of quantum chemistry. A family of cluster models have been generated based on the conceptual idea of mononuclear Cr(III) with three covalent ligands that coordinate through oxygen, as exemplified by the Cr(III)G structure earlier proposed by DeRossi *et al.*,[13] cf. Fig. 1. For the main reaction steps investigated, the various models provide consistent reaction energy profiles.

A reaction mechanism consisting of the following three reaction steps is found to be viable: (**1**) C—H activation of ethane according to σ-bond metathesis, accompanied by formation of O—H and Cr—C bonds, (**2**) β-H transfer to chromium with subsequent loss of ethene, and (**3**) regeneration of the chromium site by means of σ-bond metathesis with subsequent loss of H_2. Apart from the absence of molecular adsorption of ethane, the cycle consisting of reactions (1–3) agrees with earlier proposals.[3,37] Regeneration of the catalytic cite according to reaction (3) requires the initial C—H activation step to involve a Cr—O ester linkage to the surface. Based on free-energy calculations, the second reaction step, involving β-hydrogen transfer to the metal, is found to be rate determining. Activation free energy and enthalpy are computed in excess of 300 and 200 kJ mol^{-1}, respectively.

Based on the computed energies, an alternative mechanism is formulated in which C—H activation takes

place at a reactive hydridochromium complex formed in reaction (2) (above), rather than at more stable chromium species with three oxygen ligands. Key features of this mechanism are the formation of H—H and Cr—C bonds by means of σ-bond metathesis and that C—H activation becomes rate determining. The computed activation enthalpy is approximately $70\,kJ\,mol^{-1}$, i.e. some $130\,kJ\,mol^{-1}$ less than computed for the mechanism proposed in Refs. 3 and 37. The importance of this alternative mechanism relies on the ability to maintain a reactive hydridochromium site, i.e. to prevent formation of more stable species in which chromium is covalently bonded to three oxygen ligands. This ability is a sensitive function of the local structure about chromium. On DeRossi-type species, the water molecule formed in reaction (1) is likely to desorb, thus making reformation of the Cr—O bond less likely. On chromium species with three Cr—O ester linkages to the surface, a silanol moiety, rather than water, is made in the initial C—H/Cr—O activation. At fairly strained surface sites, the silanol can relax away from chromium, and thus hinder reformation of the Cr—O bond. On the other hand, if the silanol moiety remains loosely coordinated to chromium, one must expect facile regeneration of the Cr—O bond according to reaction (3) above.

It is conceivable that both mechanisms are at work in active catalysts. The presence of traces of moisture in the feed will terminate the hydride-based mechanism. Specific details in the drying and calcination procedures may influence the geometrical strain of mononuclear Cr(III) sites and thereby also the effective mechanism for dehydrogenation.

Acknowledgments

S. L. and K. J. B. thank the Research Council of Norway (NFR) for financial support and for a grant of computer time through the Programme for Supercomputing. M. A. and J. S. thank 'Deutsche Forschungsgemeinschaft' for support within SFB 546.

REFERENCES

1. Weckhuysen BM, Wachs IE, Schoonheydt RA. *Chem. Rev.* 1996; **96**: 3327–3349.
2. Bhasin MM, McCain JH, Vora BV, Imai TT, Pujado PR. *Appl. Catal. A Gen.* 2001; **221**: 397–419.
3. Weckhuysen BM, Schoonheydt RA. *Catal. Today* 1999; **51**: 223–232.
4. Frey FE, Huppke WF. *Ind. Eng. Chem.* 1933; **25**: 54–59.
5. McDaniel MP. *J. Catal.* 1982; **76**: 17–28.
6. Kim DS, Tatibouet JM, Wachs IE. *J. Catal.* 1992; **136**: 209–221.
7. Haukka S, Lakomaa EL, Suntola T. *Appl. Surf. Sci.* 1994; **75**: 220–227.
8. Hardcastle FD, Wachs IE. *J. Mol. Catal.* 1988; **46**: 173–186.
9. Kim DS, Wachs IE. *J. Catal.* 1993; **142**: 166–171.
10. Weckhuysen BM, Deridder LM, Schoonheydt RA. *J. Phys. Chem.* 1993; **97**: 4756–4763.
11. Weckhuysen BM, Verberckmoes AA, Buttiens AL, Schoonheydt RA. *J. Phys. Chem.* 1994; **98**: 579–584.
12. Fouad NE, Knozinger H, Zaki MI, Mansour SAA. *Z. Phys. Chem.* 1991; **171**: 75–96.
13. DeRossi S, Ferraris G, Fremiotti S, Garrone E, Ghiotti G, Campa MC, Indovina V. *J. Catal.* 1994; **148**: 36–46.
14. Lugo HI, Lunsford JH. *J. Catal.* 1985; **91**: 155–166.
15. Cimino A, Cordischi D, Febbraro S, Gazzoli D, Indovina V, Occhiuzzi M, valigi M, Boccuzzi F, Chiorino A, Ghiotti G. *J. Mol. Catal.* 1989; **55**: 23–33.
16. Cimino A, Cordischi D, DeRossi S, Ferraris G, Gazzoli D, Indovina V, Minelli G, Occhiuzzi M, Valigi M. *J. Catal.* 1991; **127**: 744–760.
17. Ashmawy FM. *J. Chem. Soc., Faraday Trans. I* 1980; **76**: 2096–2101.
18. Marcilly C, Delmon B. *J. Catal.* 1972; **24**: 336–347.
19. König P, Tétényi P. *Acta Chim. Hung.* 1976; **89**: 123–136.
20. König P, Tétényi P. *Acta Chim. Hung.* 1976; **89**: 137–150.
21. Cavani F, Koutyrev M, Trifiro F, Bartolini A, Ghisletti D, Iezzi R, Santucci A, DelPiero G. *J. Catal.* 1996; **158**: 236–250.
22. Weckhuysen BM, Bensalem A, Schoonheydt RA. *J. Chem. Soc., Faraday Trans.* 1998; **94**: 2011–2014.
23. Hakuli A, Kijtokivi A, Krause AOI, Suntola T. *J. Catal.* 1996; **161**: 393–400.
24. Hakuli A, Harlin ME, Backman LB, Krause AOI. *J. Catal.* 1999; **184**: 349–356.
25. Weckhuysen BM, Verberckmoes AA, Debaere J, Ooms K, Langhans I, Schoonheydt RA. *J. Mol. Catal. A* 2000; **151**: 115–131.
26. DeRossi S, Ferraris G, Fremiotti S, Cimino A, Indovina V. *Appl. Catal. A* 1992; **81**: 113–132.
27. DeRossi S, Casaletto MP, Ferraris G, Cimino A, Minelli G. *Appl. Catal. A Gen.* 1998; **167**: 257–270.
28. Kytokivi A, Jacobs JP, Hakuli A, Merilainen J, Brongersma HH. *J. Catal.* 1996; **162**: 190–197.
29. Hakuli A, Kytokivi A, Krause AOI. *Appl. Catal. A Gen.* 2000; **190**: 219–232.
30. Puurunen RL, Weckhuysen BM. *J. Catal.* 2002; **210**: 418–430.
31. Masson J, Bonnier JM, Duvigneaud PH, Delmon B. *J. Chem. Soc., Faraday Trans. I* 1977; **73**: 1471–1498.
32. Gorriz OF, Corberán VC, Fierro JLG. *Ind. Eng. Chem. Res.* 1992; **31**: 2670–2674.
33. DeRossi S, Ferraris G, Fremiotti S, Indovina V, Cimino A. *Appl. Catal. A Gen.* 1993; **106**: 125–141.
34. Puurunen RL, Airaksinen SMK, Krause AOI. *J. Catal.* 2003; **213**: 281–290.
35. Ghiotti G, Chiorino A. *Spectrochim. Acta A* 1993; **49**: 1345–1359.
36. Airaksinen SMK, Harlin ME, Krause AOI. *Ind. Eng. Chem. Res.* 2002; **41**: 5619–5626.
37. Burwell RL, Littlewood AB, Cardew M, Pass G, Stoddard CTH. *J. Am. Chem. Soc.* 1960; **82**: 6272–6280.
38. Stahl SS, Labinger JA, Bercaw JE. *Angew. Chem., Int. Ed. Engl.* 1998; **37**: 2181–2192.
39. Siegbahn PEM, Crabtree RH. *J. Am. Chem. Soc.* 1996; **118**: 4442–4450.
40. Frash MV, van Santen RA. *J. Phys. Chem. A* 2000; **104**: 2468–2475.
41. Frash MV, van Santen RA. *Phys. Chem. Chem. Phys.* 2000; **2**: 1085–1089.
42. Arndtsen BA, Bergman RG, Mobley TA, Peterson TH. *Acc. Chem. Res.* 1995; **28**: 154–162.
43. Corker J, Lefebvre F, Lecuyer C, Dufaud V, Quignard F, Chopli A, Evans J, Basset JM. *Science* 1996; **271**: 966–969.
44. Casty GL, Matturro MG, Myers GR, Reynolds RP, Hall RP. *Organometallics* 2001; **20**: 2246–2249.
45. Hall MB, Fan HJ. *Adv. Inorg. Chem.* 2003; **54**: 321–349.
46. Børve KJ, Espelid Ø. In *Nanostructured Catalysts*, Scott SL, Crudden CM, Jones CW (eds). Kluwer Academic: New York, 2002; *Nanostructure Science and Technology* **3**: 85–112.
47. Spuhler P, Holthausen MC, Nachtigallova D, Nachtigall P, Sauer J. *Chem.-Eur. J.* 2002; **8**: 2099–2115.
48. Nachtigallova D, Nachtigall P, Sauer J. *Phys. Chem. Chem. Phys.* 2001; **3**: 1552–1559.
49. Nachtigall P, Nachtigallova D, Sauer J. *J. Phys. Chem. B* 2000; **104**: 1738–1745.

50. Nachtigallova D, Nachtigall P, Sierka M, Sauer J. *Phys. Chem. Chem. Phys.* 1999; **1**: 2019–2026.
51. Rodriguez-Santiago L, Sierka M, Branchadell V, Sodupe M, Sauer J. *J. Am. Chem. Soc.* 1998; **120**: 1545–1551.
52. Iarlori S, Ceresoli D, Bernasconi M, Donadio D, Parrinello M. *J. Phys. Chem. B* 2001; **105**: 8007–8013.
53. Ceresoli D, Bernasconi M, Iarlori S, Parrinello M, Tosatti E. *Phys. Rev. Lett.* 2000; **84**: 3887–3890.
54. Du MH, Kolchin A, Cheng HP. *J. Chem. Phys.* 2003; **119**: 6418–6422.
55. Limoge Y. *Cr. Acad. Sci. IV-Phys.* 2001; **2**: 263–283.
56. Feuston BP, Garofalini SH. *J. Chem. Phys.* 1988; **89**: 5818–5824.
57. Vollmayr K, Binder K. *Phys. Rev. B* 1996; **54**: 15808–15827.
58. Vollmayr K, Kob W. *Ber. Bunsen. Phys. Chem.* 1996; **100**: 1399–1401.
59. Huff NT, Demiralp E, Cagin T, GoddardIII WA. *J. Non-Cryst. Solids* 1999; **253**: 133–142.
60. Sierka M, Sauer J. *Faraday Discuss.* 1997; **106**: 41–62.
61. Baerends EJ, Bérces A, Bo C, Boerrigter PM, Cavallo L, Deng L, Dickson RM, Ellis DE, Fan L, Fischer TH, Fonseca Guerra C, van Gisbergen SJA, Groeneveld JA, Gritsenko OV, Harris FE, van den Hoek P, Jacobsen H, van Kessel G, Kootstra F, van Lenthe E, Osinga VP, Philipsen PHT, Post D, Pye CC, Ravenek W, Ros P, Schipper PRT, Schreckenbach G, Snijders JG, Sola M, Swerhone D, te Velde G, Vernooijs P, Versluis L, Visser O, van Wezenbeek E, Wiesenekker G, Wolff SK, Woo TK, Ziegler T. *ADF 2000.02 Computer Code* 2000.
62. Guerra CF, Snijders JG, te Velde G, Baerends EJ. *Theor. Chem. Acc.* 1998; **99**: 391–403.
63. Vosko SH, Wilk L, Nusair M. *Can. J. Phys.* 1980; **58**: 1200–1211.
64. Perdew JP. *Phys. Rev. B* 1986; **33**: 8822–8824.
65. Becke AD. *Phys. Rev. A* 1988; **38**: 3098–3100.
66. Frisch MJ, Trucks GW, Schlegel HB, Scuseria GE, Robb MA, Cheeseman JR, Zakrzewski VG, Montgomery JA Jr, Stratmann RE, Burant JC, Dapprich S, Millam JM, Daniels AD, Kudin KN, Strain MC, Farkas O, Tomasi J, Barone V, Cossi M, Cammi R, Mennucci B, Pomelli C, Adamo C, Clifford S, Ochterski J, Petersson GA, Ayala PY, Cui Q, Morokuma K, Malick DK, Rabuck AD, Raghavachari K, Foresman JB, Cioslowski J, Ortiz JV, Baboul AG, Stefanov BB, Liu G, Liashenko A, Piskorz P, Komaromi I, Gomperts R, Martin RL, Fox DJ, Keith T, Al-Laham MA, Peng CY, Nanayakkara A, Challacombe M, Gill PMW, Johnson B, Chen W, Wong MW, Andres JL, Gonzalez C, Head-Gordon M, Replogle ES, Pople JA. *Gaussian 98, Revision A.9*. Gaussian: Pittsburgh, PA, 1998.
67. Becke AD. *J. Chem. Phys.* 1993; **98**: 5648–5652.
68. Stephens PJ, Devlin FJ, Chablowski CF, Frisch MJ. *J. Phys. Chem.* 1994; **98**: 11623–11627.
69. Bell RP. *The Tunnel effect in Chemistry*. Chapman and Hall: London, 1980.
70. Gale JD. *J. Chem. Soc., Faraday Trans.* 1997; **93**: 629–637.
71. Gale JD. *Phil. Mag. B* 1996; **73**: 3–19.
72. Binks DJ. PhD Thesis, University of Surrey 1994.
73. *Cerius*^{2} *Program, Molecular Simulations Inc.*, 9685 Scranton Road, San Diego, CA 92121, USA. 1998.
74. Sierka M, Sauer J. *J. Phys. Chem.* 2000; **112**: 6983–6996.
75. Sauer J, Sierka M. *J. Comput. Chem.* 2000; **21**: 1470–1493.
76. Hu WP, Liu YP, Truhlar DG. *J. Chem. Soc., Faraday Trans.* 1994; **90**: 1715–1725.
77. Stallons JM, Iglesia E. *Chem. Eng. Sci.* 2001; **56**: 4205–4216.
78. Mukhopadhyay AB, Oligschleger C, Dolg M. *Phys. Rev. B* 2003; **67**: Art. No. 014106.
79. Mischler C, Kob W, Binder K. *Comp. Phys. Comm.* 2002; **147**: 222–225.
80. Brinker CJ, Kirkpatrick RJ, Tallant DR, Bunker BC, Montez B. *J. Non-Cryst. Solids* 1988; **99**: 418–428.
81. Bunker BC, Haaland DM, Michalske TA, Smith WL. *Surf. Sci.* 1988; **222**: 95–118.
82. Tsuneyuki S, Tsukada M, Aoki H, Matsui Y. *Phys. Rev. Lett.* 1988; **61**: 869–872.
83. Laurence PR, Hillier IH. *Comp. Mat. Sci.* 2003; **28**: 63–75.
84. Zecchina A, Spoto G, Ghiotti G, Garrone E. *J. Mol. Catal.* 1994; **86**: 423–446.
85. Espelid Ø, Børve KJ. *J. Catal.* 2000; **195**: 125–139.
86. Airaksinen SMK, Krause AOI, Sainio H, Lahtinen J, Chao KJ, Guerroro-Péerez ML, Banãres MA. *Phys. Chem. Chem. Phys.* 2003; **5**: 4371–4377.
87. Busca G. *J. Catal.* 1989; **120**: 303–313.
88. Indovina V, Cimino A, DeRossi S, Ferraris G, Ghiotti G, Chiorino A. *J. Mol. Catal.* 1992; **75**: 305–319.